

Low-Density Aerodynamics of the Stardust Sample Return Capsule

Richard G. Wilmoth*, Robert A. Mitcheltree† and James N. Moss‡

NASA Langley Research Center, Hampton, VA 23681

The aerodynamics of the Stardust Sample Return Capsule are analyzed in the low-density, transitional flow regime using free-molecular, Direct Simulation Monte Carlo, Navier-Stokes, and Newtonian methods to provide inputs for constructing a transitional flow bridging relation. The accuracy of this bridging relation in reconstructing the aerodynamic coefficients given by the more exact methods is presented for a range of flight conditions and vehicle attitudes. There is good agreement between the various prediction methods, and a simple sine-squared bridging relation is shown to provide a reasonably good description of the axial force, normal force, and pitching moment over a range of Knudsen numbers from 0.001 to 10. The predictions show a static instability of the Stardust capsule in the free-molecular regime that persists well into the transitional flow. The addition of a thin disk to the base of the capsule is shown to remove this static instability. However, the extremely high entry velocity of 12.6 km/s for the proposed trajectory introduces difficult design issues for incorporating this disk caused by the high aerothermal loads that occur even under relatively rarefied conditions.

Nomenclature

A_{ref}	Reference area ($= \pi R_b^2$), m^2
<i>c.g.</i>	Center of gravity ($= 0.3675D_b$), m
C_A	Axial force coefficient, $F_A/(\frac{1}{2}\rho_\infty V_\infty^2 A_{ref})$
C_N	Normal force coefficient, $F_N/(\frac{1}{2}\rho_\infty V_\infty^2 A_{ref})$
C_m	Pitching moment coefficient, $M_y/(\frac{1}{2}\rho_\infty V_\infty^2 A_{ref} L_{ref})$
F_A	Axial force, N
F_N	Normal force, N
D_b	Maximum body diameter, m
Kn	Knudsen number, λ/D_b
L_{ref}	Reference length ($= D_b$), m
M	Mach number
M_y	Moment about pitch axis, N-m
n	Number density, $1/m^3$
P	Pressure, N/m^2
q	Heat flux, W/m^2
R_a	Afterbody base radius, m
R_b	Maximum body radius, m
R_n	Nose radius, m
R_s	Shoulder radius, m
S	Distance along body, m
T	Temperature, K
V	Velocity, m/s
x, y, z	Cartesian body axes, m
α	Angle of attack, deg
λ	Mean free path, m

ρ	Mass density, kg/m^3
τ	Shear stress, N/m^2
θ_a	Afterbody half-cone angle, deg
θ_f	Forebody half-cone angle, deg

Subscripts

<i>cg</i>	Center of gravity
<i>cont</i>	Continuum
<i>fm</i>	Free molecular
∞	Freestream

Introduction

STARDUST is a NASA Discovery-class mission designed to make a close encounter with the comet Wild-2, collect samples of dust and volatiles within the coma and return them to Earth.¹ The Earth return will use a trajectory that produces an entry velocity of approximately 12.6 km/s. Landing footprint restrictions require accurate knowledge of the aerodynamics of the reentry capsule throughout the trajectory from the free-molecular flow regime of initial atmospheric encounter to the subsonic regime just prior to landing. The high entry velocity makes the size of the landing footprint somewhat more sensitive to the low-density aerodynamics than typical reentries from low Earth orbit. More importantly, aerodynamic instabilities in the low-density regime can cause angle-of-attack excursions that produce undesirable capsule attitudes at peak heating conditions.

The low-density aerodynamics of entry vehicles are frequently determined through the use of free-molecular and Newtonian methods with bridging relations to define the transitional flow aerodynamics.^{2,3} These bridging relations typically use the Knudsen number as the independent parameter and require knowledge of the Knudsen number above which molecular collisions can be neglected (free-molecular) and

*Aerospace Engineer, Aerothermodynamics Branch, Aero- and Gas-Dynamics Division, Senior Member AIAA.

†Aerospace Engineer, Aerothermodynamics Branch, Aero- and Gas-Dynamics Division, Senior Member AIAA.

‡Aerospace Engineer, Aerothermodynamics Branch, Aero- and Gas-Dynamics Division, Fellow AIAA.

Copyright ©1997 by the American Institute of Aeronautics and Astronautics, Inc. No copyright is asserted in the United States under Title 17, U.S. Code. The U.S. Government has a royalty-free license to exercise all rights under the copyright claimed herein for governmental purposes. All other rights are reserved by the copyright owner.

the Knudsen number below which the flow may be treated as a continuum. The aerodynamic coefficients in the free-molecular and continuum limits are also required. In many instances, this approach produces estimates of the aerodynamic coefficients that are sufficiently accurate especially when combined with active or passive flight control that has sufficient margins for correcting entry trajectory and attitude. However, because of the need for increased accuracy for the passively-controlled Stardust Sample Return Capsule (SRC), a study was conducted in which both direct simulation Monte Carlo (DSMC) and Navier-Stokes calculations were used to accurately define the transitional aerodynamics.

The purpose of this paper is to discuss the methodology and present the results used to define the low-density aerodynamic database for the SRC. A description of the methodology used to define the complete aerodynamic database from hypersonic, free-molecular to subsonic, continuum flow is given in a companion paper.⁴ Aerodynamic drag based on free-molecular, 2D and 3D DSMC, Newtonian, and 2D and 3D Navier-Stokes methods is used to establish the Knudsen number limits of the transitional flow regime and thereby the appropriate bridging relation parameters. Further 3D DSMC analyses are then used to establish the validity of the bridging relations for predicting other aerodynamic coefficients including the pitching moments needed to determine static stability. Finally, since the baseline configuration exhibits a static instability, additional free-molecular and DSMC results are shown for a modified geometry representing one possible remedy to the static instability.

Geometry

The baseline geometry of the Stardust Sample Return Capsule is shown in Figure 1 and consists of a 60-deg half-angle, spherically-blunted cone forebody with a 30-deg half-angle conical afterbody. The nose radius, R_n , is 0.2286 m, the shoulder radius, R_s , is 0.01905 m, and the overall diameter, D_b , is 0.8128 m. The afterbody base has a radius of 0.2116 m. The center of gravity of the baseline configuration is 0.2987 m aft of the nose ($x_{cg}/D_b = 0.3675$). This aft location results in a static instability in the free-molecular flow regime. One approach to removing this instability without moving the center of gravity is analyzed which has a thin circular disk or “skirt” added to the afterbody base as shown in Figure 2. The diameter of this disk is the same as the overall diameter of the forebody, 0.8128 m. The thickness of the disk was not set by the design at the time of analysis, but for the purpose of this analysis was assumed to have a thickness of 0.0015 m.

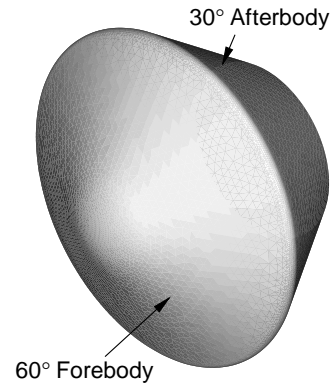


Fig. 1 Baseline geometry of Stardust Sample Return Capsule.

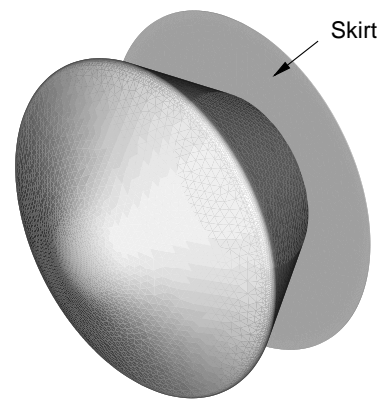


Fig. 2 Modified geometry with afterbody skirt.

Trajectory/Flight Conditions

A nominal reentry trajectory was determined from 3 degree-of-freedom analyses,⁴ and specific trajectory points selected for detailed analysis are given in Table 1. Because of the small size of the capsule, atmospheric interface denoting the beginning of the transitional flow regime occurs at a relatively low altitude. For this trajectory, free-molecule flow is expected at altitudes above about 130 km, and fully continuum flow is expected at altitudes below about 80 km. Axisymmetric DSMC calculations were performed for all trajectory points given in Table 1 at zero degrees angle of attack. Full 3D DSMC calculations were performed for all points except the lowest altitude at zero degrees and for altitudes of 134.75, 100.9 and 83.68 km at angles of attack of 10 and 30 deg. Axisymmetric Navier-Stokes calculations were performed for an altitude of 83.68 km at 0 deg. and full 3D Navier-Stokes calculations were performed for angles of attack of 0 and 10 deg. Additional Navier-Stokes calculations were performed at several altitudes lower than those in the table for development of the complete aerodynamic database.⁴

Table 1 Flight Conditions for Entry Simulations

Altitude, km	Velocity, m/s	Number Density, 1/m ³	Mole Fractions			T_∞ , K	T_w , K	Knudsen Number	Mach Number
			O ₂	N ₂	O				
134.75	12,597.1	1.48832x10 ¹⁷	0.0659	0.6716	0.2625	577.23	400	12.8	23.96
120.45	12,607.7	5.93941x10 ¹⁷	0.0845	0.7327	0.1828	381.15	500	2.92	30.27
100.90	12,620.2	1.09988x10 ¹⁹	0.1768	0.7844	0.0388	199.37	1,000	0.136	43.94
92.00	12,618.5	4.98474x10 ¹⁹	0.2056	0.7873	0.0071	202.05	1,200	0.0301	44.10
83.68	12,591.5	1.77978x10 ²⁰	0.2385	0.7615	0.0000	216.54	1,500	0.00857	42.68
75.98	12,486.8	5.73854x10 ²⁰	0.2385	0.7615	0.0000	218.14	1,800	0.00266	42.17

Computational Methods

Bridging Relation

The form of the bridging relation used in this study is:

$$C_A = C_{A,cont} + (C_{A,fm} - C_{A,cont}) \sin^2(\phi) \quad (1)$$

where

$$\phi = \pi (a_1 + a_2 \log_{10} Kn) \quad (2)$$

Here, C_A represents the axial force coefficient, but similar expressions are used for other aerodynamic coefficients. The quantities $C_{A,cont}$ and $C_{A,fm}$ represent the values of the coefficient in the continuum and free-molecular limits respectively. The constants a_1 and a_2 are determined by choosing Knudsen numbers corresponding to each of these limits. While general guidelines frequently give these limits to be $Kn=0.01$ for the continuum limit and $Kn=10.0$ for the free-molecular limit, it has been shown that both of these limits frequently need to be extended to achieve fully continuum or fully free-molecular flow.^{2,5} Furthermore, since the constants, a_1 and a_2 , are simply adjustable parameters in Eqn. 1, they should be adjusted to give the best overall description of the transitional flow aerodynamics when additional data are available.

In this study, free-molecular, DSMC, Navier-Stokes, and Newtonian calculations are used to define the behavior of the axial-force coefficient throughout the transitional regime. The constants, a_1 and a_2 , are determined to give the best overall match to the computed C_A at $\alpha = 0^\circ$. Continuum and free-molecular values are then computed for all aerodynamic quantities (axial force, normal force, and pitching moment coefficients) over a range of α and used together with the constants a_1 and a_2 to provide a complete aerodynamic database. To verify the adequacy of the bridging relations for non-zero incidence angles, full 3D DSMC calculations are performed for the selected incidence angles and trajectory points described previously.

Free-Molecular and DSMC Analyses

Free-molecular analyses were initially performed for the baseline configuration using standard free-molecular aerodynamic relations applied to a discretized surface geometry. However, the concave shape

of the modified geometry that later needed to be addressed made the use of typical line-of-sight shadowing somewhat suspect. Therefore, the results denoted free-molecular in this paper were actually calculated using DSMC with molecular collisions disabled. Comparisons of the free-molecular results with the collisionless DSMC for the baseline configuration (which has no concavities) show that the two methods give aerodynamic coefficients that agree to within less than 1%.

DSMC analyses used the standard algorithm developed by Bird.⁶ Axisymmetric analyses were performed using the standard G2 code⁷ and full 3D analyses were performed using a relatively new code called DAC developed by LeBeau.⁸ The 3D code uses an unstructured triangular grid to represent the surface geometry together with a two-level embedded Cartesian grid for the flowfield. Gas collisions are modeled using the variable hard-sphere (VHS) model and the Larsen-Borgnakke model for internal energy exchange. Gas-surface interactions are assumed to be fully diffuse with full energy accommodation to the surface temperature. The surface temperature is based on an approximate heat transfer estimate and a simple radiative-equilibrium analysis and is given in Table 1 for each of the trajectory points analyzed. In general, both the axisymmetric and 3D analyses model the gas as 5-species reacting air using a 23-equation reaction set. However, for the lowest altitude cases with the 3D code, it was necessary to use a parallel version of the DAC code in which chemistry is not yet implemented. Therefore, some limited comparisons were made between 3D calculations with and without chemistry based on relatively coarse grids for angles of attack up to 30 deg. These comparisons show that while there is considerable dissociation of O_2 and N_2 for both the 100.9 and 83.68 km cases, this dissociation has a negligible effect on the aerodynamics. Therefore, the 3D results presented at 83.68 km were calculated without considering chemical reactions.

Navier-Stokes and Newtonian Analyses

Navier-Stokes analyses are performed using the Langley Aerothermodynamics Upwind Relaxation Algorithm (LAURA) CFD code.^{9,10} LAURA is an upwind-bias, point-implicit relaxation algorithm for obtaining the numerical solution to the Navier-Stokes equations

for three dimensional, viscous, hypersonic flows in thermochemical nonequilibrium. It has been used to describe the aerodynamics of several blunt bodies similar to the Stardust Sample Return Capsule including Mars Pathfinder.¹¹ Calculations were performed at the trajectory point corresponding to the lowest altitude given in Table 1 (as well as several lower altitudes given in Ref. 4 for the continuum portion of the trajectory) with no-slip boundary conditions imposed. The LAURA results are used to establish the magnitude of the aerodynamic coefficients at the Knudsen number corresponding to the continuum limit. Newtonian analysis is then used to provide the variations of these coefficients with angle of attack relative to the LAURA results.

Results

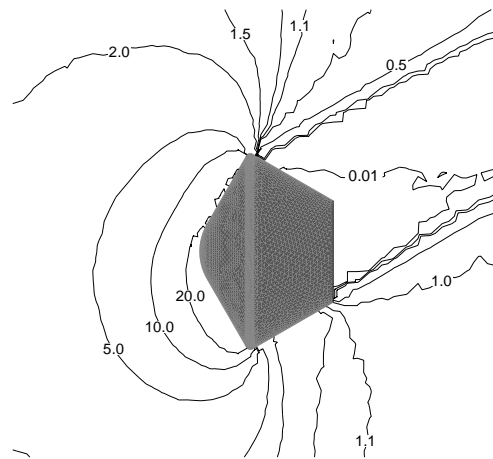
Flowfields

Number density contours for three different trajectory points at $\alpha = 30^\circ$ are shown in Figure 3 to illustrate the changing character of the flowfield as the degree of rarefaction changes. At 135 km, the flow is essentially free molecular and while there is a significant increase in density in front of the vehicle, there is no distinct shock behavior. As the density increases at the lower altitudes, a shock layer becomes more evident until at 83 km, a very distinct bow shock is produced, and the flow does not expand in the wake to densities as low relative to the freestream as it does at the higher altitudes.

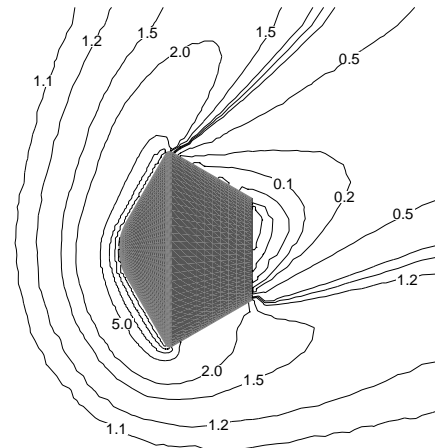
Baseline Geometry Aerodynamics

Figure 4 shows a comparison of the axial force coefficient computed by the various methods as a function of Knudsen number for $\alpha = 0^\circ$. There is generally good agreement between the 2D (axisymmetric) and 3D DSMC methods as well as the Navier-Stokes results at $Kn=0.00857$. The bridging relation is found to give a reasonable fit to the computed results by choosing $Kn=0.001$ as the continuum limit and $Kn=10$ as the free-molecular limit. The lower limit is reduced by a factor of 10 below that value normally considered to represent the start of continuum flow. The DSMC results indicate that the free-molecular limit should perhaps be increased, but it was felt that more weight should be given to the lower Knudsen numbers where the aerodynamic forces are greater and have more influence on the trajectory. Other forms of bridging relations might also give a better fit to the data.^{2, 5}

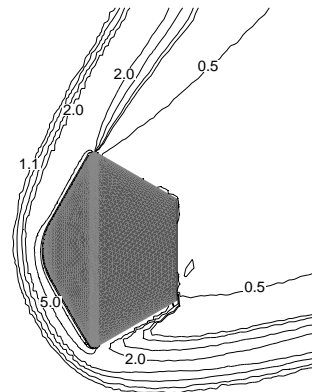
One reason the predicted results do not follow the current bridging relation better is that the points chosen follow a computed trajectory where the vehicle velocity and atmospheric properties are changing as well as the atmospheric density. Furthermore, the surface temperature increases significantly over the range of conditions studied. While the dominant change in aerodynamic properties is caused by the change in



a) 135 km.



b) 101 km.



c) 83 km.

Fig. 3 Number density contours (n/n_∞) at various altitudes. $\alpha = 30^\circ$.

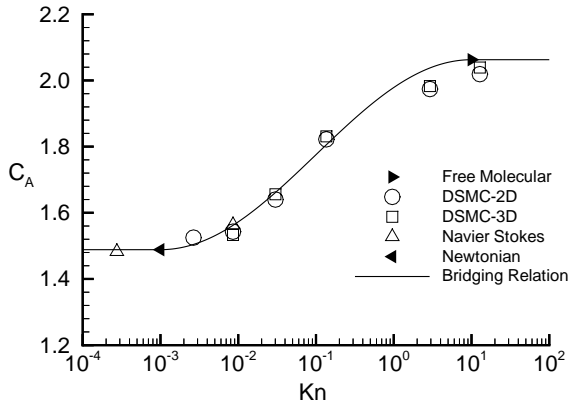
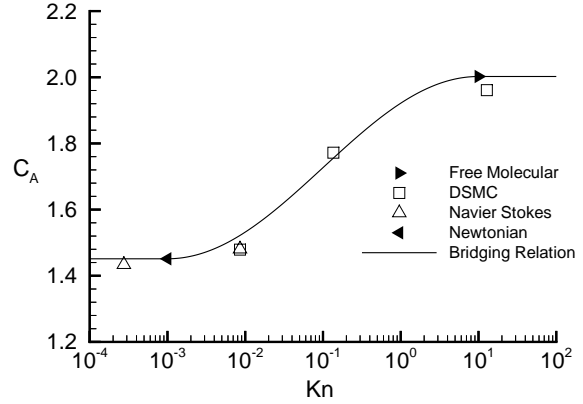


Fig. 4 Axial force coefficient for the baseline geometry, $\alpha = 0^\circ$.

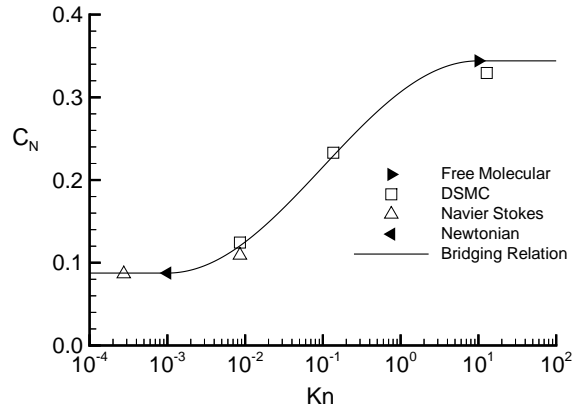
density, small variations in the vehicle velocity, atmospheric temperature and composition, and surface temperature produce small changes in aerodynamics as well. Since the bridging relation only correlates the aerodynamic properties to the Knudsen number which is essentially just the inverse of the number density, changes in the other variables (which are included in the DSMC and Navier-Stokes simulations) are not taken into account except at the free-molecular and continuum endpoints. The sensitivity to trajectory variables other than density can be computed at the free-molecular condition, and it is estimated that variations of up to about 5% can be attributed to changes in velocity and surface temperature along the more rarefied portion of the trajectory. These variations are sufficient to cause the computed behavior to deviate somewhat from sine-squared behavior of the bridging relation. While this deviation is not considered significant for the Stardust trajectory, it may be worthwhile to investigate alternate bridging methodology for other entry trajectories.

Based on the results in Figure 4, the constants in Eqn. 2 were set to $a_1 = 3/8$ and $a_2 = 1/8$. These constants were used to determine the other aerodynamic coefficients at non-zero angles of attack with the free-molecular and continuum values of these coefficients adjusted appropriately. A comparison of the bridging relation predictions to DSMC and Navier-Stokes results for C_A , C_N and $C_{m,cg}$ is shown in Figure 5 for $\alpha = 10^\circ$. There is good agreement between the DSMC, Navier-Stokes and bridging relation predictions of C_A and C_N , but the DSMC values tend to be higher than both the Navier-Stokes and bridging relation values for $C_{m,cg}$ at the lower Knudsen number. At the $Kn=0.00857$, the grid for the DSMC calculation was not resolved to within one mean free path near the vehicle surface as it was for the higher Knudsen numbers. A limited grid sensitivity study showed that refining the grid would reduce the value of $C_{m,cg}$ slightly, but the resources required to fully resolve the Knudsen layer for this flight condition were not jus-

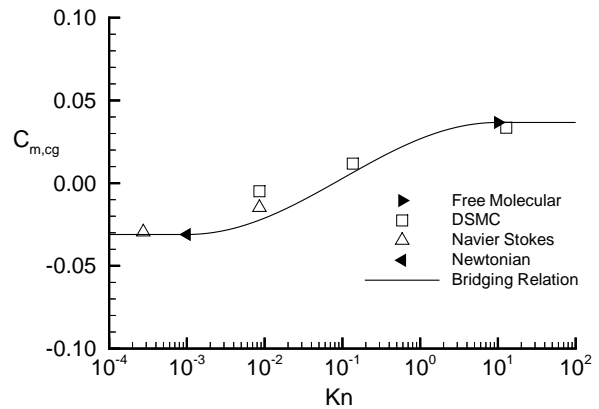
tifiable for a preliminary design study. Furthermore, $C_{m,cg}$ is very sensitive to small errors in C_N at low angles of attack, and the difference in C_N between the DSMC and Navier-Stokes results is less than 1% of the total force on the vehicle.



a) Axial force, C_A .



b) Normal force, C_N .



c) Pitching moment, $C_{m,cg}$.

Fig. 5 Comparison of bridging relation predictions to DSMC and Navier-Stokes predictions, $\alpha = 10^\circ$.

The aerodynamics of the baseline geometry over a wide range of angles of attack is shown in Figure 6. The bridging relation is used to provide the complete

angle-of-attack results and the DSMC and Navier-Stokes results are included for comparison. In general, the bridging relation gives a good match to the DSMC and Navier-Stokes results for the three aerodynamic coefficients shown. Figure 6(c) also demonstrates that the vehicle exhibits a static instability in the free-molecular regime ($Kn=12.8$), approaches neutral stability at $Kn=0.136$, and is stable with a trim angle of 0° near the hypersonic continuum. Although the free-molecular result actually has a trim point at slightly over 60° , such a large trim angle is undesirable because it would require substantially greater thermal protection on the afterbody of the vehicle. Furthermore, the stability near this trim point is marginal, and the vehicle could trim in a backward position ($\alpha = 180^\circ$) where it is statically stable. Even with the addition of a reasonable amount of spin stabilization (doubling the spin rate from 5 rpm to 10 rpm), six-degree-of-freedom simulations have shown that undesirable excursions in angle of attack are possible as the vehicle approaches peak heating conditions. Therefore, a modification to the design was considered that would achieve greater aerodynamic stability in the transitional regime.

Modified Geometry Aerodynamics

One concept proposed for stabilizing the Stardust vehicle in the free-molecular regime is the addition of a “skirt” or disk attached to the afterbody base as shown in Figure 2. Free-molecular (“collisionless” DSMC) calculations were performed for both the baseline and modified geometries over an angle-of-attack range of 0° to 180° , and the pitching moment results are shown in Figure 7. The addition of the skirt not only provides static stability with a trim angle of $\alpha = 0^\circ$, but also makes the vehicle statically unstable at $\alpha = 180^\circ$ thus eliminating the possibility of the vehicle remaining in a backward position as it enters the atmosphere.

However, the presence of the afterbody skirt causes undesirable heating and aerodynamic effects in the continuum regime. Therefore, a design was considered that removes the skirt after the vehicle passes through the unstable portion of the transitional regime. A bridging relation was constructed that uses the aerodynamics of the modified geometry for the free-molecular limit and the aerodynamics of the baseline geometry (without the skirt) in the continuum limit. In figure 8, a comparison of this modified bridging relation and the DSMC results for the fully-skirted geometry at $Kn=0.136$ shows good agreement between the two and demonstrates static stability with a trim angle of zero.

It should be noted that the use of “collisionless” DSMC to simulate free-molecular flow theoretically provides more accurate results than a traditional free-molecular analysis based on line-of-sight techniques. The collisionless DSMC fully accounts for the thermal velocity spread which can produce higher forces on

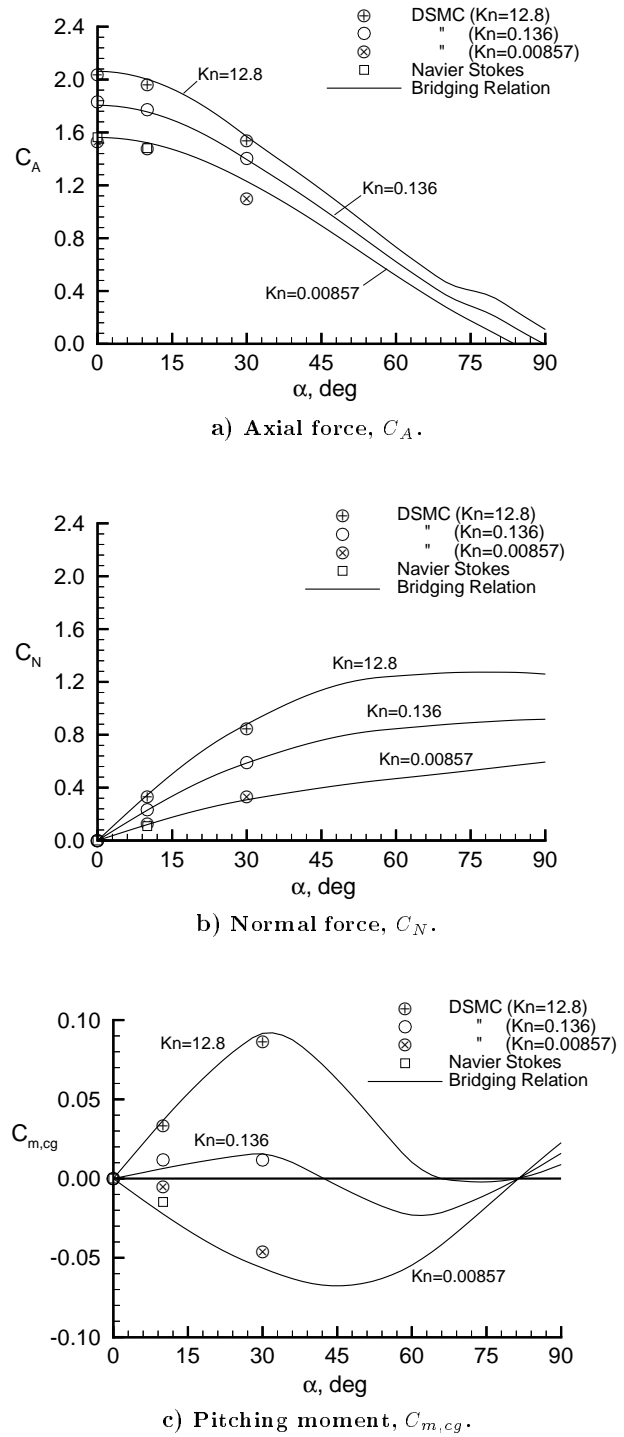


Fig. 6 Aerodynamics of the baseline geometry.

“hidden” surfaces than the analytical techniques, and these forces can become non-negligible at lower Mach numbers. Furthermore, the particle-tracing techniques used in DSMC account for multiple surface collisions, and these multiple collisions may be important for concave surfaces such as the skirted geometry. A direct measure of this effect is obtained by comparing the collisionless DSMC axial force coefficient for the two geometries at $\alpha = 0^\circ$. For the unskirted ge-

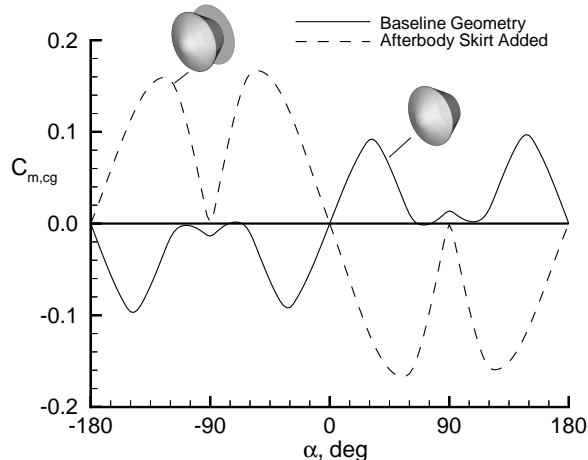


Fig. 7 Pitching moment for the baseline and modified geometries in the free-molecular regime.

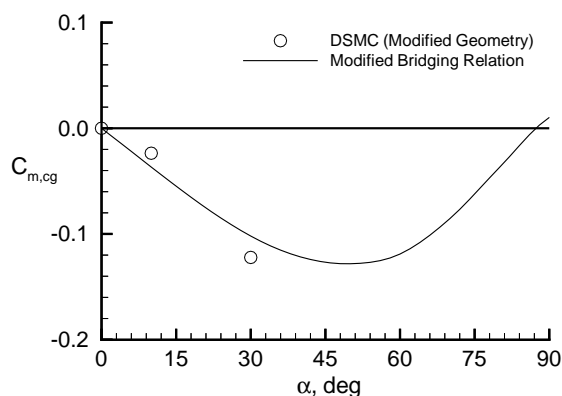


Fig. 8 Pitching moment for the bridging relation modified to use a combination of baseline and modified geometry aerodynamics, $Kn=0.136$.

ometry, $C_A = 2.063$, while for the skirted geometry, $C_A = 2.112$. Based on a simple line-of-sight free-molecular analysis for an infinite Mach number, the two values would be the same. While this difference is not large, it serves to point out the need to account for concavities if the most accurate results are desired.

Flowfield and Surface Properties for Baseline and Modified Geometries

To design an afterbody skirt such that the skirt will survive the portion of the trajectory where it is needed but will effectively “fail” or be removed due to aerothermal loads after passing through the transitional regime requires detailed knowledge of the forces and heat transfer on the skirt itself. Since the skirt should survive at least to the point where the unmodified baseline geometry has neutral stability, it was decided to use DSMC to estimate the loads and heating on the skirt at $Kn=0.136$.

It is instructive to first examine the differences in flowfield structures between the baseline and skirted

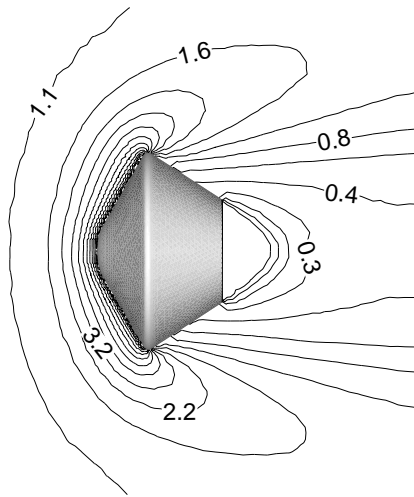
geometries. Figure 9 shows comparisons of the density and flow streamlines for both geometries at zero degrees angle of attack. The larger wake produced by the skirt is expected. However, it is also seen that the densities in the concave region adjacent to the afterbody are significantly higher with the skirt. Although the overall flow is fairly rarefied, the densities in the concavity are sufficiently high that there is significant recirculation as shown by the streamlines. This stagnation-like behavior has a marked effect on the afterbody forces and heating as well as on the skirt.

Figure 10 shows the pressure, friction (shear stress), and heat transfer along the body for the baseline and skirted geometries as a function of the distance, S , along the surface. As expected the skirt has no effect on these quantities along the forebody, but produces a marked increase in the forces and heat transfer along the afterbody. Furthermore, the peak forces and heat transfer at the outermost edges of the skirt approach magnitudes comparable to those on the forebody. These high forces and heating even at this moderately rarefied flow make the task of selecting a skirt material and design very difficult. The skirt must survive up to and perhaps slightly beyond this flight condition, withstand significant heating along the outer edges, retain sufficient structural integrity to provide the aerodynamic stability, and then be removed from the vehicle before reaching the hypersonic continuum. While the aerodynamic characteristics of the skirted geometry are much better than the baseline geometry, these design issues coupled with other design constraints make this solution impractical at the present time.

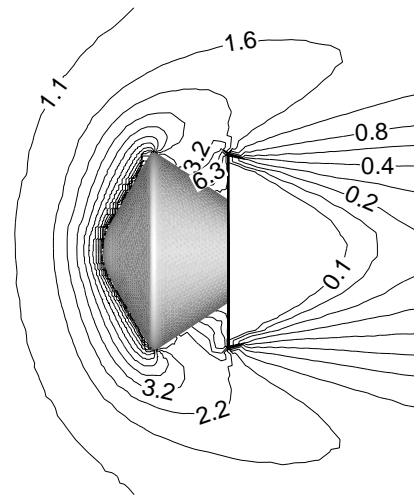
Concluding Remarks

DSMC and Navier-Stokes computations have been used to assist in constructing accurate engineering methods based on bridging relations to predict the aerodynamics of the Stardust Sample Return Capsule in the low-density transitional flow regime. Bridging relations provide the ability to develop a more complete database that is needed for six-degree-of-freedom trajectory simulations. A simple sine-squared form for the bridging relation fits the data computed by the more exact methods reasonably well and meets the criteria needed for Stardust trajectory simulations. Improvements to the overall methodology may be needed to provide better representation of the aerodynamics in the most rarefied portion of the transitional flow regime where benchmark calculations are required but the present methodology is adequate for preliminary design studies.

The baseline Stardust configuration has been shown to exhibit a static instability in the free-molecular regime that persists well into the transitional flow portion of the trajectory. Eliminating this instability poses a particular challenge because of the high entry

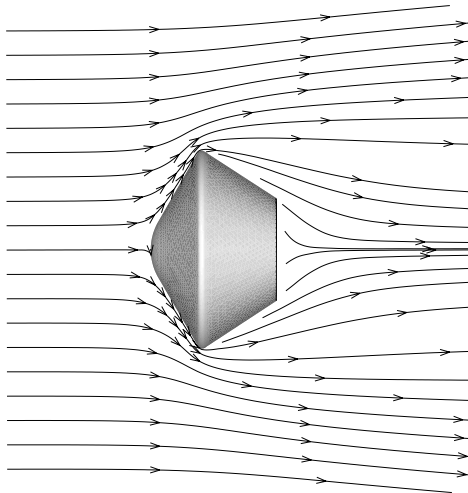


Baseline Geometry

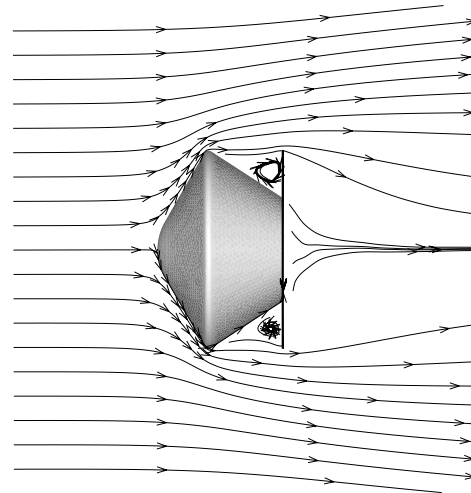


Afterbody Skirt Added

a) Number density (n/n_∞) contours.



Baseline Geometry



Afterbody Skirt Added

b) Streamlines.

Fig. 9 DSMC-computed flowfields for baseline and modified geometries, $\text{Kn}=0.136$, $\alpha = 0^\circ$.

velocity as well as other design constraints. The addition of a simple disk-shaped afterbody skirt readily achieves the goal of aerodynamic stability but introduces new aerothermal design problems that must be thoroughly addressed to determine its feasibility. Since no database exists for such a design and since no appropriate flight data are available at such high entry velocities, the use of computational methods is essential. Since many of these issues occur in the rarefied portion of the trajectory, accurate DSMC analyses are especially important.

Acknowledgements

G. J. LeBeau of NASA Johnson Space Center provided the DAC 3D DSMC code. Prasun Desai of NASA Langley Research Center performed the 6-DOF simulations that revealed the dynamic instability in the transitional regime.

References

- ¹Atkins, K. L., Brownlee, D. E., Duxbury, T., Yen, C., and Tsou, P., "STARDUST: Discovery's Interstellar Dust and Cometary Sample Return Mission," *Proceedings from the 1997 IEEE Aerospace Conference*, 1997.
- ²Blanchard, R. C., "Rarefied Flow Lift-to-Drag Measurements of the Shuttle Orbiter," *ICAS Proceedings 1986*, edited by P. Santini and R. Staufenbiel, Vol. II, London, UK, 1986, pp. 1421-1430.
- ³Ivanov, M. S., Markelov, G. N., Gimelshein, S. F., and Antonov, S. G., "DSMC Studies of High-Altitude Aerodynamics of Reentry Capsule," *20th International Symposium on Rarefied Gas Dynamics*, Beijing, China, Aug. 1996.
- ⁴Mitcheltree, R. A., Wilmoth, R. G., Cheatwood, F. M., Brauckmann, G. J., and Greene, F. A., "Aerodynamics of Stardust Sample Return Capsule," *AIAA Paper 97-2304*, Jun. 1997.
- ⁵Celenligil, M. C., Moss, J. N., and Blanchard, R. C., "Three-Dimensional Rarefied Flow Simulations for the Aeroassist Flight Experiment," *AIAA Journal*, Vol. 29, No. 1, Jan. 1991, pp. 52-57.
- ⁶Bird, G. A., *Molecular Gas Dynamics and the Direct Simulation of Gas Flows*, Clarendon Press, Oxford, 1994.
- ⁷Bird, G. A., *The G2/A3 Program Users Manual*, G.A.B. Consulting Pty Ltd, Killara, N.S.W., Australia, Mar. 1992.
- ⁸Wilmoth, R. G., LeBeau, G. J., and Carlson, A. B., "DSMC Grid Methodologies for Computing Low-Density Hypersonic Flows About Reusable Launch Vehicles," *AIAA Paper 96-1812*, Jun. 1996.
- ⁹Gnoffo, P. A., Gupta, R. N., and Shinn, J. L., "Equations and Physical Models for Hypersonic Air Flows in Thermal and Chemical Nonequilibrium," *NASA TP 2867*, Feb. 1989.
- ¹⁰Gnoffo, P. A., "An Upwind-Biased, Point-Implicit Relaxation Algorithm for Viscous, Compressible Perfect-Gas Flows," *NASA TP 2953*, Feb. 1990.
- ¹¹Braun, R. D., Powell, R. W., Englund, W. C., Gnoffo, P. A., Weilmuenster, K. J., and Mitcheltree, R. A., "Mars Pathfinder Six-Degree-of-Freedom Entry Analysis," *J. of Spacecraft and Rockets*, Vol. 32, No. 6, Nov.-Dec. 1995, pp. 993-1000.

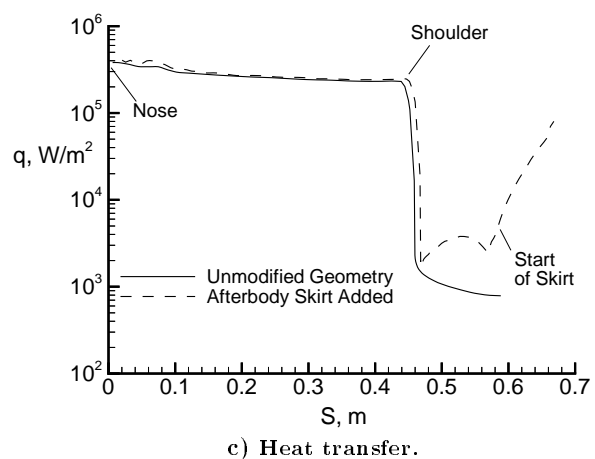
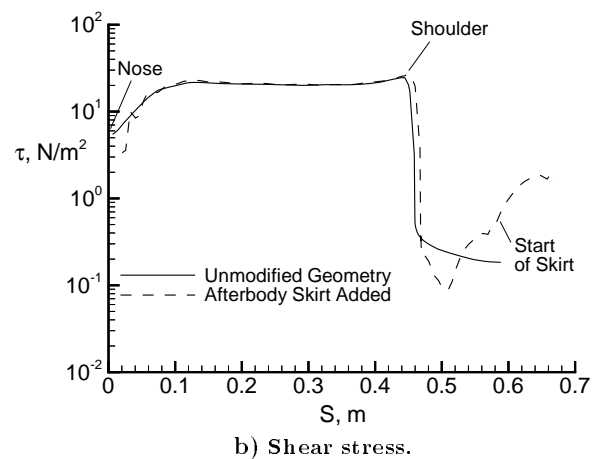
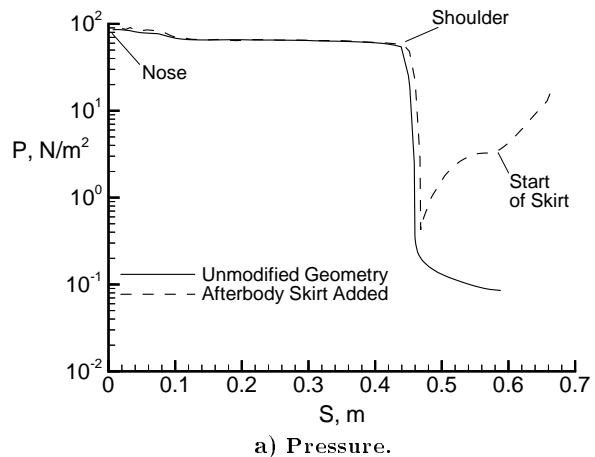


Fig. 10 DSMC-computed surface properties for baseline and modified geometries, $Kn=0.136$, $\alpha = 0^\circ$.